

Interannual Variation of the Madden–Julian Oscillation during Austral Summer

HARRY H. HENDON

NOAA/CIRES Climate Diagnostics Center, Boulder, Colorado

CHIDONG ZHANG

*Division of Meteorology and Physical Oceanography, Rosentiel School of Marine and Atmospheric Sciences,
University of Miami, Miami, Florida*

JOHN D. GLICK

NOAA/CIRES Climate Diagnostic Center, Boulder, Colorado

(Manuscript received 30 June 1998, in final form 15 October 1998)

ABSTRACT

Interannual variability of the Madden–Julian oscillation (MJO), the dominant mode of intraseasonal variability in the Tropics, is investigated during the extended austral summer season November–March, which is when the MJO is most prominent. Indexes of the level of MJO activity are developed using outgoing longwave radiation and zonal wind analyses at 850 mb for 1974–98. Based on these indexes, interannual variations in the level of MJO activity are found to be primarily associated with changes in the number of discrete MJO events each year and with changes in the intensity of intraseasonal convection across the Indian and western Pacific Oceans, where the MJO is normally prominent. An eastward shift of MJO activity east of the date line does occur during El Niño events. However, the overall level of MJO activity is found to be uncorrelated with El Niño, except during exceptional warm events when MJO activity is diminished. The level of MJO activity is shown to be weakly related to sea surface temperature anomalies in the equatorial Indian and western Pacific Oceans, but the weak correlations imply that much of the year-to-year variability of the MJO is internally generated, independent of any slowly varying boundary forcing. Such year-to-year variations of the intensity of the MJO are, however, associated with changes in the distribution of seasonal mean convection across the tropical Indian and western Pacific Oceans. This interannual variation of convection unrelated to SST variability may thus act as a limit to seasonal predictions that rely heavily on equatorial Pacific SST anomalies.

1. Introduction

This study is aimed at understanding interannual variability of tropical intraseasonal convection. Particular focus is given to year-to-year variations of the Madden–Julian oscillation (MJO; e.g., Madden and Julian 1972), which is the dominant mode of intraseasonal convective variability in the Tropics. While a precise definition of the MJO will be given in section 3, here it will suffice to note that the MJO refers to a planetary-scale disturbance in both convection and circulation (predominantly zonal wind), which propagates eastward along the equator across the Indian and western Pacific Oceans with a period of 40–50 days and a local wavelength there of about 20 000 km. It is most prominent during late austral spring and summer (e.g., Madden 1986; Wang and Rui

1990) but exhibits large year-to-year variations in intensity (e.g., Gutzler and Madden 1989; Salby and Hendon 1994; Anyamba and Weare 1995).

The present study will focus on interannual variations of MJO activity during November through March, recognizing that intraseasonal activity with similar frequency and spatial scale occurs during boreal summer in the Asian–Indian monsoon (e.g., Lau and Chan 1986; Gadgil and Asha 1992). However, intraseasonal convective activity during boreal summer exhibits pronounced poleward propagation in the Indian Ocean, with only limited eastward propagation (e.g., Wang and Rui 1990) and much less coherence with planetary-scale, eastward-propagating circulation anomalies (e.g., Salby and Hendon 1994). Furthermore, when records of zonal wind and outgoing longwave radiation (OLR, which is a proxy for tropical convection) that span the entire year are analyzed, the dominant tropical intraseasonal mode that emerges is the eastward-propagating, austral summer MJO (e.g., Lau and Chan 1988;

Corresponding author address: Harry Hendon, Climate Diagnostics Center, 325 Broadway, R/E/CD, Boulder, CO 80303.
E-mail: hhh@cdc.noaa.gov

Salby and Hendon 1994; Anyamba and Weare 1995; Zhang and Hendon 1997).

Understanding interannual variability of the MJO is of practical importance because of the role of the MJO in a number of phenomena. For example, the MJO affects onset and breaks of the Australian summer monsoon (e.g., Hendon and Liebmann 1990), while the level of MJO activity in a given summer may be inversely related to the cumulative monsoon rainfall (Holland 1986). The relatively weak but spatially coherent zonal surface stress anomalies produced by the MJO are largely responsible for exciting the Kelvin waves that dominate intraseasonal variability of the thermocline in the equatorial Pacific (e.g., Kessler et al. 1995; Hendon et al. 1998). These waves may cause a rectified zonal displacement of the eastern edge of the Pacific warm pool (Kessler et al. 1995) and may play an active role in the onset and demise of some El Niño–Southern Oscillation (ENSO) events (e.g., Lau and Chan 1988). There is also growing evidence that the surface flux variations associated with strong MJO events play an important role in maintenance of the mean state of the tropical Pacific warm pool (e.g., Ralph et al. 1997).

Previous studies of the interannual variation of tropical intraseasonal variability have emphasized the relationship with ENSO. For instance, Gutzler (1991) showed that a 40–50-day variance of lower-tropospheric zonal wind tends to increase at equatorial stations near and east of the date line and decrease at stations in the far western Pacific during warm ENSO conditions. A similar result was found by Fink and Speth (1997) using OLR variance. However, these studies did not explicitly examine the impact on coherent eastward-propagating activity, which appears to be the variability relevant to monsoon variability and air–sea interaction in the western Pacific. Slingo et al. (1999), who used the variance of intraseasonally filtered zonal mean zonal wind at 200 mb as an indirect measure of globally integrated MJO activity, found no significant relationship between the strength of MJO activity and ENSO, or with any other sea surface temperature (SST) anomaly for that matter. Measures of the level of MJO activity that explicitly discriminate to spatially coherent, eastward-propagating phenomena also apparently do not show a systematic relationship with ENSO. For instance, Salby and Hendon (1994) developed a measure of MJO activity based on wavenumber-frequency filtering of equatorial OLR, zonal wind, and tropospheric temperature. The level of MJO activity was seen to be below normal during both the 1982–83 warm event and the 1988–89 cold event, but above normal during the 1984–85 cold event. Furthermore, large year-to-year variations in eastward-propagating MJO activity were observed during non-ENSO years. Anyamba and Weare (1995), who used a form of empirical orthogonal function (EOF) analysis to extract the dominant eastward-propagating, intraseasonal mode of tropical convection, detected similar behavior.

An example of year-to-year variations of MJO activity unrelated to ENSO is illustrated in Fig. 1, which displays Hovmöller plots of OLR averaged between 5°N and 10°S for October–March 1989/90 and 1990/91. Neither of these years exhibited sea surface temperature anomalies associated with the extremes of ENSO. During 1989/90, intraseasonal variation of convection was dominated by two well-defined episodes of planetary-scale eastward propagation from the western Indian Ocean to near the date line. In contrast, only a hint of organized eastward propagation during late October through November is evident in 1990–91. Rather, the intraseasonal variation of convection during this year was dominated by quasi-stationary fluctuations at the longitudes of the Australian summer monsoon.

The goal of the present study is to further quantify the year-to-year variations of eastward-propagating MJO activity, typified in Fig. 1, and to explore the extent that the interannual variations can be related to SST anomalies (associated with ENSO and otherwise), which may alter the normal distribution of near-equatorial convective activity. Such an analysis will provide insight into the predictability of organized convective activity across the Indian and Pacific Oceans based on knowledge of the sea surface temperature and the degree to which interannual anomalies of intraseasonal activity develop unrelated to slowly varying boundary conditions.

2. Data

Interannual variability of the MJO is assessed here primarily with OLR, which is a widely used proxy for tropical convection. Because the main emphasis here is on coherent eastward-propagating convection that occurs predominantly during austral summer, this study is restricted to the extended austral summer season, November through March. Daily OLR on a 2.5° grid are available from 1974 through April 1998 (Liebmann and Smith 1996). Because most of 1978 is missing, only 22 complete November through March seasons are available for this period.

Most of the analyses here are carried out on intraseasonally filtered data. The intraseasonal filter was accomplished by first extending the November through March records for each year by an additional 15 days at each end, in order to accommodate application of a window. The least-square quadratic fit to each segment was then removed, which effectively removes the annual cycle and its interannual variance (e.g., Ferranti et al. 1990). The first and last 15 days of each segment were then tapered with a cosine-tapered rectangular window. Each segment was then Fourier transformed. Frequencies corresponding to periods of 30 to 90 days were retained by application of a triangular-tapered rectangular window (half power at 30 and 90 days) and finally inverse transformed. Subsequent means and variances

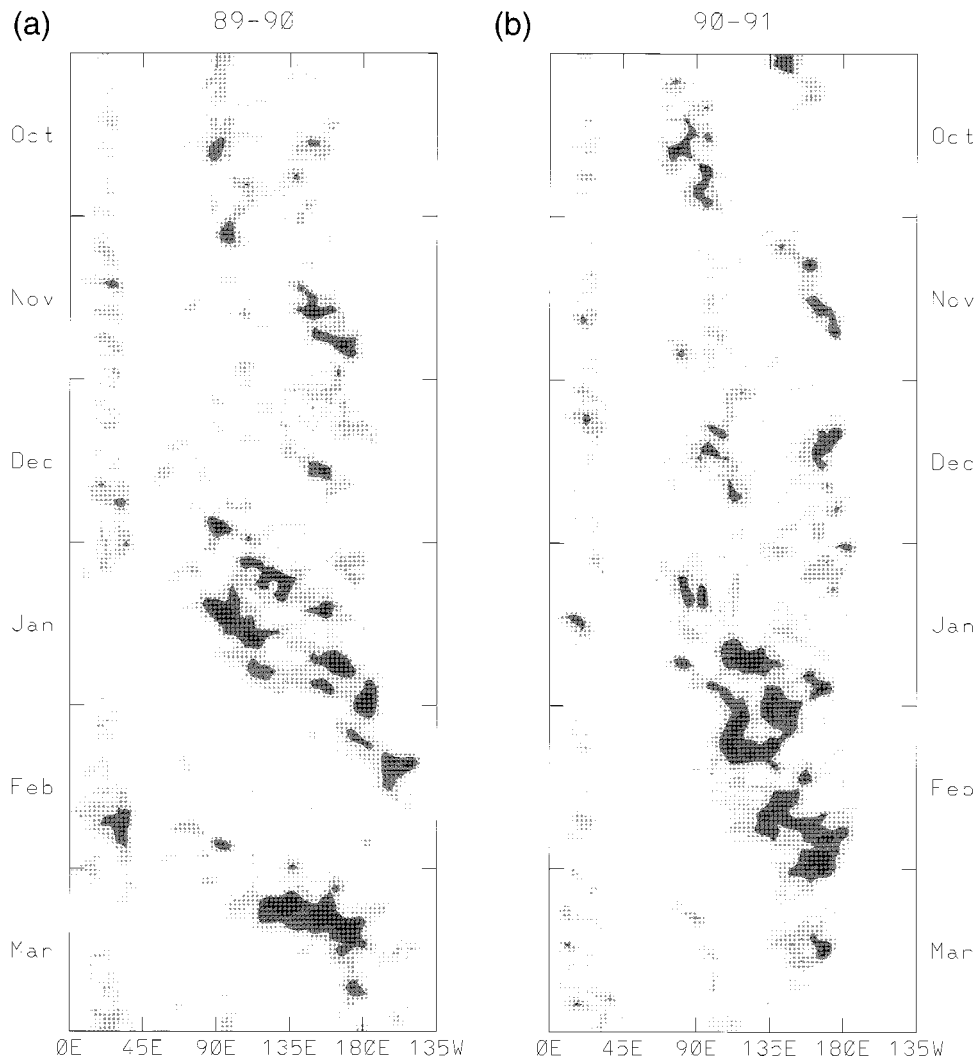


FIG. 1. Longitude-time sections of daily OLR (shaded for values less than 225 W m^{-2} , shading interval 10 W m^{-2}) for (a) Oct 1989–Mar 1990, and (b) Oct 1990–Mar 1991. OLR was averaged latitudinally 5°N – 10°S and low-pass filtered with one pass of a 1–2–1 running mean.

from this intraseasonally filtered data were formed with the November through March values (i.e., the first and last 15 days of each segment, which were subjected to windowing, were discarded).

Monthly mean SST for the period 1974–98 on a 2.5° grid are also employed. Prior to 1982, these data are derived from reconstructed monthly mean SSTs (Smith et al. 1996), based on in situ observations interpolated with EOFs onto a 2° grid. Beginning in 1982, these data are derived from monthly averages of weekly SST analyses (Reynolds and Smith 1994) that are based on optimum interpolation (OI) of in situ and satellite observations on a 1° grid. Linear interpolation is used to put both the reconstructed and OI SST analyses onto a 2.5° grid. The state of ENSO is diagnosed here using a Niño3

SST index, which is formed by averaging monthly SST in the domain 5°N – 5°S , 150° – 90°W .

A primary limitation of this study of interannual variability is the relatively short record length employed (i.e., 22 yr). This limitation is especially important when relationships between measures of the level of MJO activity and SST are explored. To add some confidence to the relationships found here based on OLR, a similar record of zonal wind at 850 mb from the NCEP (National Centers for Environmental Prediction) reanalyses (Kalnay et al. 1996) is also employed. We choose to use zonal wind at 850 mb because it exhibits many of the same characteristics of the MJO as does OLR (e.g., Salby and Hendon 1994; see below). The 200-mb zonal wind from the NCEP reanalyses is also used to construct

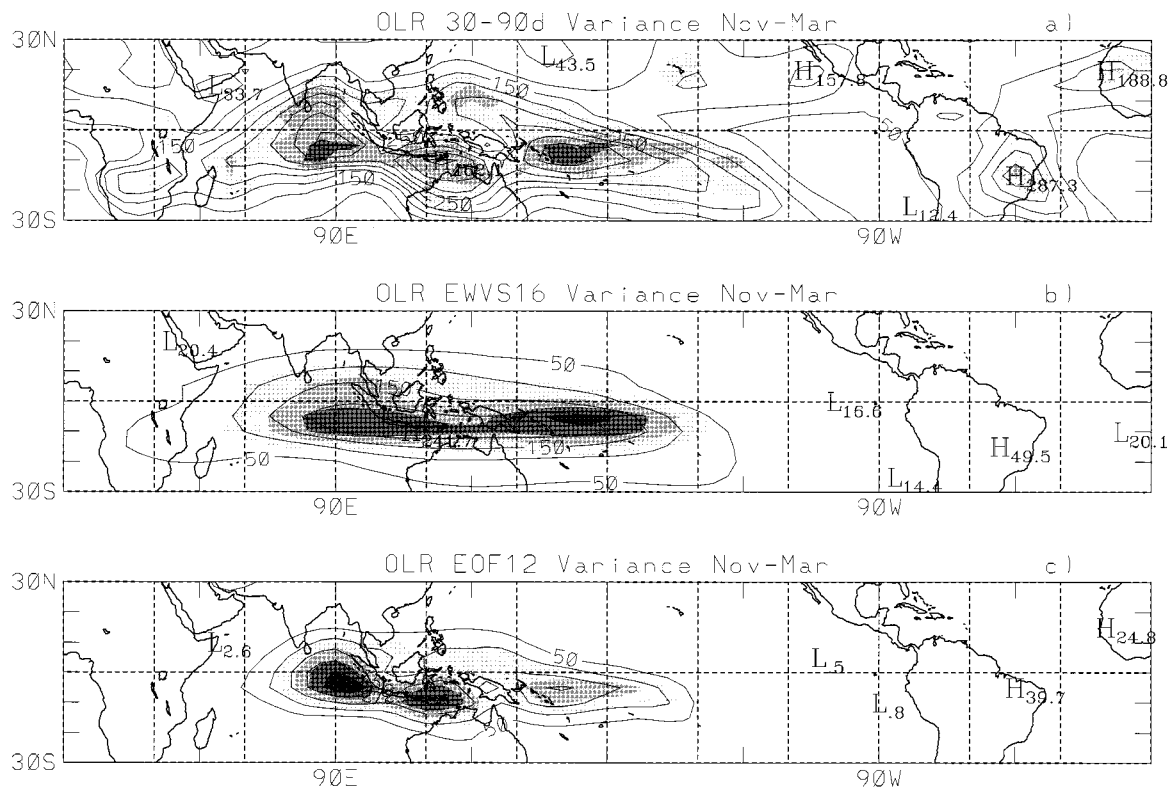


FIG. 2. Variance (contour interval $50 \text{ W}^2 \text{ m}^{-4}$) of (a) 30–90-day filtered OLR, (b) OLR_{EWVS} , and (c) OLR_{EOF} averaged for Nov through Mar 1974–1998. The respective interannual standard deviations are shaded. Shading increment in (a) is $50 \text{ W}^2 \text{ m}^{-4}$, in (b) and (c) is $25 \text{ W}^2 \text{ m}^{-4}$.

the zonal mean zonal wind index of MJO activity discussed by Slingo et al. (1999).

3. Measures of the MJO

Measures of the intensity of the MJO are required that capture the salient features of the MJO. These include the concentration of intraseasonal convective variance across the Indian and western Pacific Oceans (Fig. 2a) and at low eastward wavenumbers with a near 50-day period (Fig. 3a). The first measure of the MJO in convection is based simply on wavenumber-frequency filtering of OLR, similar to that done by Salby and Hendon (1994). Here, the frequency range corresponds to periods 30–90 days for eastward wavenumbers 1–6. This range of zonal wavenumbers is broader than that used by Salby and Hendon so that interannual zonal displacements of variance can be better captured. Hereafter, this wavenumber-frequency filtered OLR is referred to as OLR_{EWVS} . The distribution of variance of OLR_{EWVS} (Fig. 2b) reveals that about half of the intraseasonal convective variance across the Indian and western Pacific Oceans (Fig. 2a) is due to coherent eastward propagation, which is consistent with other estimates of the MJO signal strength based on the coherence of OLR between the Indian and western Pacific Oceans (e.g., Weickmann et al. 1985; Salby and Hendon 1994).

The second measure of the MJO is based on EOF analysis of OLR, which has been successfully used to extract the dominant mode of eastward-propagating convection associated with the MJO (e.g., Lau and Chan 1988; Ferranti et al. 1990; Zhang and Hendon 1997). Here, EOF analysis is performed on the intraseasonally filtered OLR in the entire domain 30°N–30°S. The first 10 eigenvalues, along with estimates of their sampling errors (North et al. 1982), are given in Table 1. The first two EOFs, which explain about 20% of the intraseasonal variance for this domain, are not separable, while their principal components correlate at 0.73 at a 12-day lag. Taken together, they describe an eastward-propagating disturbance with an approximately 50-day period. Their eigenvectors (not shown, but see, e.g., Ferranti et al. 1990) depict variability with a local zonal wavenumber-2 structure, concentrated just south of the equator across the Indian and western Pacific Oceans and extending eastward into the South Pacific convergence zone. Hereafter, OLR reconstructed from these two leading EOFs will be referred to as OLR_{EOF} .

The spatial distribution of variance associated with OLR_{EOF} is shown in Fig. 2c. While similar to that of OLR_{EWVS} , the EOF-based measure exhibits more detail across the Indian and western Pacific Oceans, capturing three local maxima as opposed to two broad ones. The

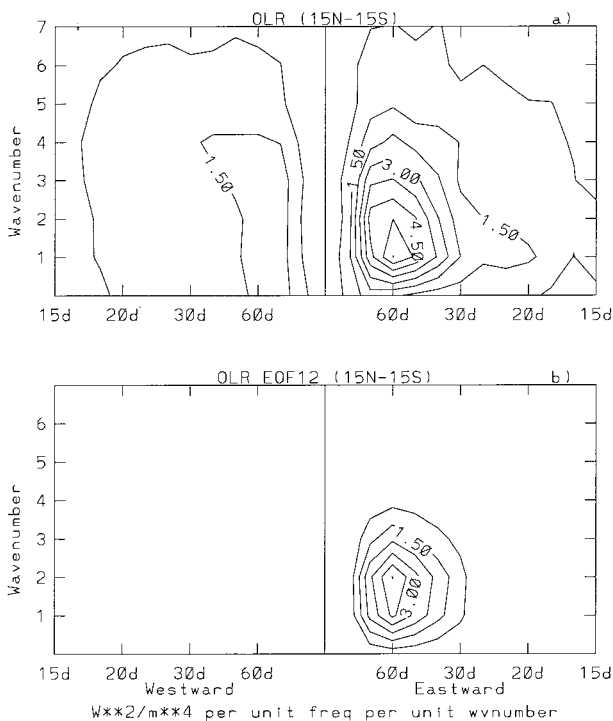


FIG. 3. Wavenumber-frequency spectra of (a) detrended OLR and (b) OLR_{EOF} . Power was computed at individual latitudes $15^{\circ}N-15^{\circ}S$, for each extended austral summer season (Nov–Mar) and then averaged. Contour interval is $0.75 W^2 m^{-4}$ per unit frequency per unit wavenumber. The abscissa is linear in frequency but labeled in the equivalent period in days.

space–time spectrum of OLR_{EOF} (Fig. 3b) indicates that this EOF-based measure efficiently captures the bulk of the eastward-propagating variance that stands out above the broad background spectrum (see also Zhang and Hendon 1997).

Similar filtering techniques are also applied to the zonal wind at 850 mb in order to assess the reliability of the signals provided by the OLR. Figure 4a displays the spatial distribution of intraseasonally filtered variance of the eddy zonal wind. Removal of the zonal mean prior to computing the variance highlights the localized intraseasonal variability produced by the MJO across the Eastern Hemisphere. There, the distribution of variance is similar to that of OLR (Fig. 2a). However, large intraseasonal variance also occurs in the extratropical storm tracks, particularly in the Northern Hemisphere, which is unrelated to MJO activity. The space–time spectrum of the equatorial eddy zonal wind (not shown) is also similar to that of OLR, but with more of a concentration of power at eastward wavenumber 1, which reflects the broader dynamical structure of the MJO in response to the spatially confined convective forcing (Salby and Hendon 1994).

Nonetheless, the same broad wavenumber–frequency filter as applied to the OLR is applied to the zonal wind to create U_{EWVS} . The spatial distribution of variance of

TABLE 1. First 10 eigenvalues (expressed as a percentage of explained variance) from the EOF analysis of intraseasonally filtered OLR in the domain $30^{\circ}N-30^{\circ}S$ for extended austral summer (Nov–Mar) 1974–98. The sampling range was estimated following North et al. (1982), assuming 66 degrees of freedom (3 possible independent samples of the MJO in each of the 22 summer seasons).

	Eigenvalue (% variance)	Range
1	10.0	11.7–8.3
2	9.3	10.9–7.7
3	5.1	5.9–4.2
4	4.1	4.8–3.4
5	2.9	3.4–2.4
6	2.7	3.1–2.3
7	2.3	2.7–1.9
8	2.2	2.6–1.8
9	2.2	2.6–1.8
10	2.0	2.3–1.7

U_{EWVS} (Fig. 4b) is concentrated over the Indian and western Pacific Oceans, where, similar to that for OLR, it locally accounts for about half of the total intraseasonal variance. The EOF-based measure was also formed using the zonal wind. However, because unrelated variance in the storm tracks extends so far into low latitudes, we found it necessary to limit the domain of the EOF analysis to $15^{\circ}N-15^{\circ}S$ in order to extract the dominant mode of tropical variability related to the MJO. As for OLR, the leading two EOFs of eddy zonal wind, which together explain 35% of the intraseasonal variance, compared to 20% for the OLR (due to the more limited latitudinal domain and to the removal of the zonal mean), are a pair, and their principal components correlate at 0.68 at a 12-day lag. Together they depict an eastward-propagating disturbance across the equatorial Indian and western Pacific Oceans. Hereafter, the zonal wind reconstructed from these two leading EOFs¹ will be referred to as U_{EOF} . The spatial distribution (Fig. 4c) and the space–time spectrum [not shown, but similar to that shown by Zhang and Hendon (1997)] of the variance of U_{EOF} show that the EOF analysis indeed discriminates to eastward-propagating variance, predominantly at wavenumbers 1 and 2, localized across the equatorial Indian and western Pacific Oceans.

While the wavenumber–frequency filter and EOF analysis appear to capture equivalent behavior, there are differences in their attributes that may have bearing on depiction of interannual variations of the MJO. The greatest attribute of the EOF analysis is that it does not presuppose the spatial structure of the MJO; it is de-

¹ Note that the zonal wind is reconstructed for the entire domain $30^{\circ}N-30^{\circ}S$ despite the fact that the EOF analysis was only carried out in the subdomain $15^{\circ}N-15^{\circ}S$. Reconstruction of the zonal wind poleward of 15° was accomplished by multiple linear regression onto the two leading principal components. Equatorward of 15° , this technique gives the same result as reconstruction directly from the two eigenvectors and their respective principal components.

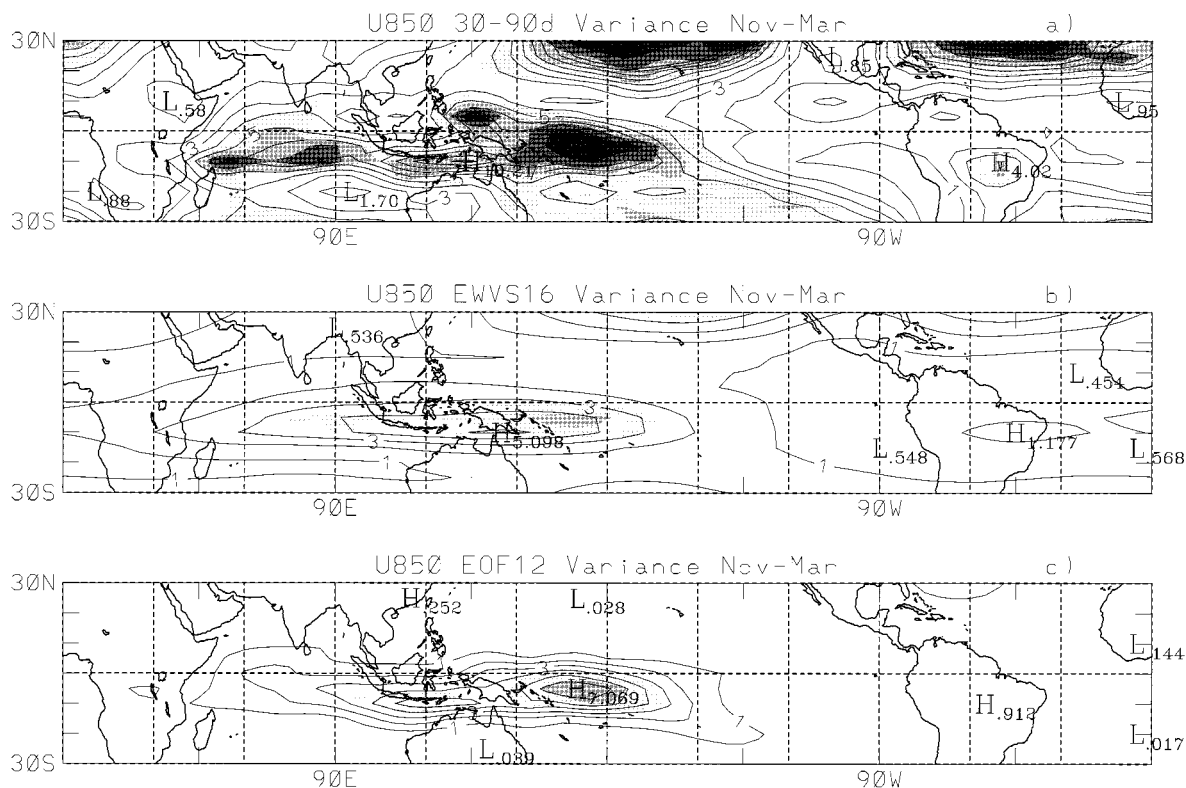


FIG. 4. As in Fig. 2 except for zonal wind variance at 850 mb. Contour interval for variance is $1 \text{ m}^2 \text{ s}^{-2}$. Shading increment for the interannual standard deviations is $1 \text{ m}^2 \text{ s}^{-2}$.

terminated objectively. However, as only two EOFs are used, the spatial structure is essentially prescribed, and the spatial distribution of variance will not vary appreciably from year to year. On the other hand, the wave-number-frequency filter, while subjectively determined, can readily capture longitudinal shifts, if any, of eastward-propagating MJO activity. As will be shown in section 4, interannual variations in the level of MJO activity result primarily from changes in the level of MJO activity across the Indian and western Pacific Oceans, where the MJO is normally prominent, and are not related to large zonal displacements of activity. Hence, both measures adequately depict the year-to-year variations.

Limited comparison is also made to the zonal mean zonal wind index proposed by Slingo et al. (1999). They argue that intraseasonally filtered (e.g., 30–90 day) zonal mean zonal wind at 200 mb, averaged from 10°N to 10°S [hereafter $[u_{30-90d}]$] is a simple index of the MJO that overcomes the concerns raised above, because equatorial zonal mean zonal wind fluctuations result from zonally integrated effects of the MJO. However, despite the fact that equatorial zonal mean zonal wind at 200 mb exhibits a dramatic spectral peak at 30–90 days [not shown, but similar to that for global angular momentum; e.g., Fig. 1 of Hendon (1995)], the MJO still only accounts for $\sim 60\%$ of the intraseasonal variance of

$[u_{30-90d}]$, as judged by the amount of power in the 30–90-day spectral peak standing above the broad red background. Hence, up to 40% of the variance of $[u_{30-90d}]$ is unrelated to the MJO. We thus prefer the use of the direct measures of the MJO based on identification of episodes of coherent eastward propagation. Nonetheless, interannual variability of the MJO depicted by $[u_{30-90d}]$ is similar to that captured by the direct measures of activity (see below) and thus confirms the utility of this simple measure.

4. Interannual variation of the MJO

In order to quantify year-to-year variations in the level of MJO activity, indexes are formed by globally averaging the variance of OLR_{EOF} and OLR_{EWVS} at each grid point between 15°N and 15°S for extended austral summer (November through March) of each year, {hereafter $[\text{OLR}_{\text{EOF}}^2]$ and $[\text{OLR}_{\text{EWVS}}^2]$, respectively}. The variances of U_{EWVS} and U_{EOF} are similarly averaged to create $[U_{\text{EWVS}}^2]$ and $[U_{\text{EOF}}^2]$, respectively. The time series of these indexes for each extended summer are shown in Fig. 5. Also shown is the mean variance of $[u_{30-90d}]$ {hereafter $[u_{30-90d}]^2$ }. All of these indexes of MJO activity exhibit similar interannual variation (see also Salby and Hendon 1994; Anyamba and Weare 1995; and Slingo et al. 1998). All four indexes based explicitly on

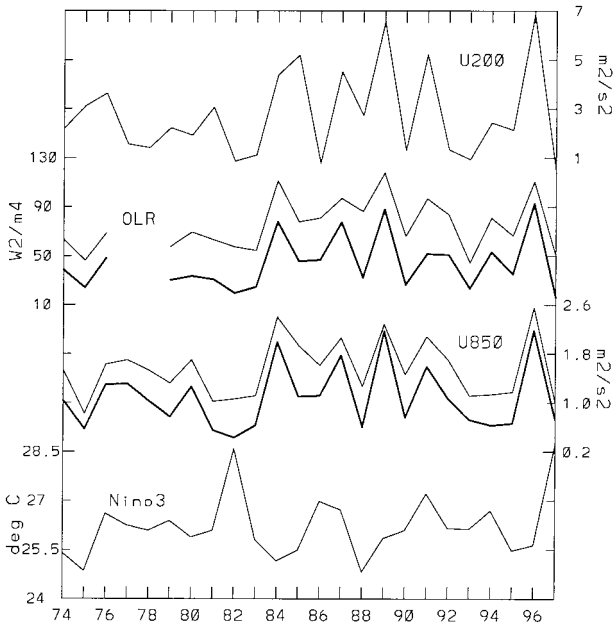


FIG. 5. Time series of (top to bottom) $[u_{30-90d}]^2$, $[\text{OLR}_{\text{EOF}}^2]$ (dark curve) and $[\text{OLR}_{\text{EWVS}}^2]$, $[U_{\text{EOF}}^2]$ (dark curve) and $[U_{\text{EWVS}}^2]$, and Niño3 SST averaged during Nov–Mar. The units for OLR variance (on left) are $\text{W}^2 \text{m}^{-4}$, for zonal wind variance (on right) are $\text{m}^2 \text{s}^{-2}$, and for Niño3 SST (on right) are $^{\circ}\text{C}$.

eastward-propagating activity correlate with each other at about 0.9 (Table 2), while they correlate with the zonal mean zonal wind index at about 0.78. This smaller correlation is consistent with the notion that upward of 40% of the variance of $[u_{30-90d}]^2$ is unrelated to the MJO.

a. Changes in characteristics of the MJO

We next examine how the year-to-year variations in the intensity of the MJO, depicted in Fig. 5, relate to changes in the characteristics of the MJO. First we examine how the number of discrete MJO events and their characteristic period vary each year. To do so, we count the number of local maxima of the first two principal components from the EOF analysis of OLR that exceed at least one standard deviation (both positive and negative). By dividing this count by 4 (one for each positive and negative phase of the two principal components), we arrive at an estimate of the total number of events each year (bold curve in Fig. 6). This number ranges

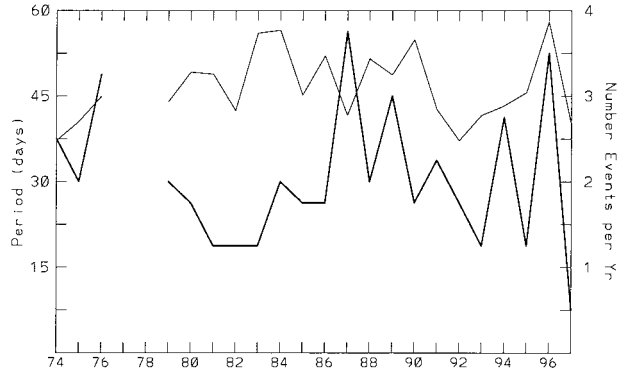


FIG. 6. Time series of number of discrete MJO events during Nov–Mar each year (bold curve; units on rhs). The thin curve is an estimate of the typical period of the MJO each year (units: days on lhs).

from a high of about 3.5 in 1996/97 to a low of about 0.5 in 1997/98 and closely tracks the mean intensity variation depicted in Fig. 5 {correlation of 0.78 with $[\text{OLR}_{\text{EOF}}^2]$ and 0.65 with $[\text{OLR}_{\text{EWVS}}^2]$ }. Hence, years of stronger than normal MJO activity tend to be years of increased number of discrete events.

The duration of each event is estimated by summing the number of days that each principal component remains greater than 71% of any maximum value that exceeds one standard deviation. If each maxima were associated with an exactly periodic event, then an estimate of a quarter-period ($-\frac{1}{8}$ cycle to $+\frac{1}{8}$ cycle) is obtained. The total number of days per each positive and negative maxima of the two principal components that exceeds this threshold (not shown) also closely tracks the variation of intensity of the MJO each year {correlation of 0.83 with $[\text{OLR}_{\text{EOF}}^2]$ and 0.76 with $[\text{OLR}_{\text{EWVS}}^2]$ }. Hence, not unexpectedly, years of greater than normal MJO activity tend to be years with a greater number of active days.

Finally, an estimate of the typical period each year is obtained by dividing the total number of active days each year by the total number of events per year (i.e., by the bold curve in Fig. 6). The typical period so estimated (thin curve in Fig. 6) ranges from a high of about 58 days in 1996–97 to a low of about 36 days in 1992–93. Such a variation of period agrees with a subjective examination of Hovmöller plots of OLR for each year. A weak relationship between the typical period and the intensity of the MJO is evident {correlation of

TABLE 2. Correlations between indexes of MJO activity and Niño3 SST for extended austral summer (Nov–Mar) 1974–75 through 1997–98. “Niño3–” signifies correlations computed with the two large El Niño years 1982–83 and 1997–98 excluded.

	$[\text{OLR}_{\text{EWVS}}^2]$	$[\text{OLR}_{\text{EOF}}^2]$	$[U_{\text{EWVS}}^2]$	$[U_{\text{EOF}}^2]$	$[u_{30-90d}]^2$
$[\text{OLR}_{\text{EOF}}^2]$	0.93				
$[U_{\text{EWVS}}^2]$	0.88	0.89			
$[U_{\text{EOF}}^2]$	0.85	0.91	0.95		
$[u_{30-90d}]^2$	0.76	0.80	0.76	0.78	
Niño3	-0.20	-0.22	-0.19	-0.15	-0.34
Niño3–	0.08	0.12	0.11	0.13	-0.07

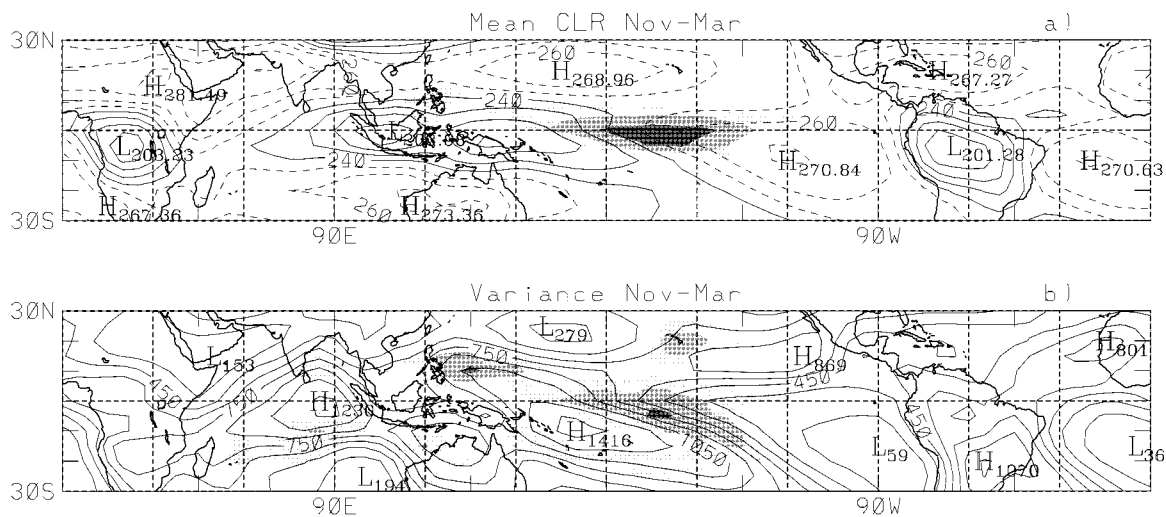


FIG. 7. Nov–Mar (a) mean OLR and (b) subseasonal variance. Contour interval in (a) is 10 W m^{-2} with values greater than 240 W m^{-2} dashed. Contour interval in (b) is $150 \text{ W}^2 \text{ m}^{-4}$. Shading in (a) indicates the interannual standard deviation of the mean OLR (shading levels begin at 8, 12, 16, and 20 W m^{-2}). Shading in (b) indicates the interannual standard deviation of OLR variance (shading levels begin at 150, 225, 300, and $375 \text{ W}^2 \text{ m}^{-4}$).

0.29 with $[\text{OLR}_{\text{EOF}}^2]$ and 0.43 with $[\text{OLR}_{\text{EWS}}^2]$, such that years of greater intensity tend to be years with longer period. However, these correlations are only marginally significant, indicating that little confidence can be placed in this relationship.

The above analysis suggests that the intensity of the MJO varies year to year primarily because of changes in the numbers of discrete events. We now examine how the geographical distribution of MJO activity varies year to year and how this relates to changes in intensity of the MJO. Shading in Figs. 2 and 4 indicates the interannual standard deviation of the respective intraseasonal variances of OLR and zonal wind at 850 mb. For all cases, maximum interannual standard deviation of these intraseasonal variances is coincident with the location of the maxima of the mean variances. While such a coincidence is expected for OLR_{EOF} and U_{EOF} , because they only include two spatial degrees of freedom, it is not necessarily required for OLR_{EWS} and U_{EWS} , or for the intraseasonally filtered OLR and zonal wind at 850 mb. Hence, this coincidence indicates that interannual fluctuations in the level of MJO activity occur primarily in conjunction with fluctuations of intraseasonal convection where the mean intraseasonal variance is normally large across the equatorial Indian and western Pacific Oceans and is not associated with significant spatial shifts of activity, particularly in the zonal direction. This behavior is in marked contrast to the mean OLR (Fig. 7a) and the total subseasonal (i.e., mean and quadratic trend from each year removed but otherwise unfiltered) OLR variance (Fig. 7b). Both the mean OLR and the total subseasonal variance exhibit maximum interannual standard deviation displaced well to the east of the maxima of their respective means, which reflects

the large eastward shift of convective activity during ENSO.

This lack of large spatial displacement of intraseasonal convective variance associated with interannual variations in the level of MJO activity, inferred from Figs. 2 and 4, is quantified by regressing seasonal mean intraseasonal OLR variance onto the time series of $[\text{OLR}_{\text{EWS}}^2]$.² Figure 8a shows this regression scaled for a one standard deviation anomaly of $[\text{OLR}_{\text{EWS}}^2]$. Enhanced MJO activity coincides with enhanced intraseasonal convective activity across equatorial Africa and south of the equator across the Indian and western Pacific Oceans, and Brazil. These are regions where intraseasonal variance is normally large and thus indicates, consistent with the examination of the interannual standard deviation relative to the distribution of mean intraseasonal variance (Fig. 2), that interannual variations of coherent eastward-propagating convection occur primarily in regions where this activity is normally large.

Figure 8b displays the regression of seasonal mean intraseasonally filtered 850-mb zonal wind variance onto $[\text{OLR}_{\text{EWS}}^2]$. Consistent with the variations of intraseasonal convective variance, enhanced MJO activity occurs in conjunction with enhanced intraseasonal zonal wind variance across the regions of normally large intraseasonal variance (equatorial Africa and the Indian and western Pacific Oceans, and, to a lesser degree, Brazil). Again, little indication of an eastward shift of

² Regressions onto $[\text{OLR}_{\text{EOF}}^2]$, $[U_{\text{EOF}}^2]$, and $[U_{\text{EWS}}^2]$ are similar due to their large mutual correlations (Table 2).

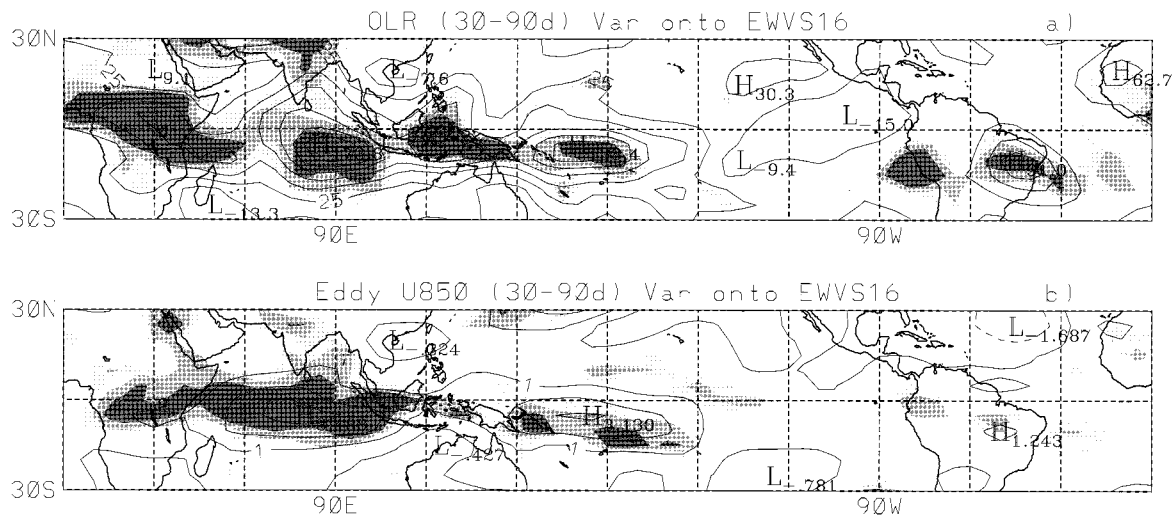


FIG. 8. (a) Regression of Nov–Mar mean 30–90-day filtered OLR variance onto $[\text{OLR}_{\text{EWVS}}^2]$. Anomalies of filtered OLR variance are shown for a 1.5 std dev anomaly of $[\text{OLR}_{\text{EWVS}}^2]$ (contour interval $25 \text{ W}^2 \text{ m}^{-4}$). Shading indicates magnitude of the correlation between filtered OLR variance and $[\text{OLR}_{\text{EWVS}}^2]$ beginning at 0.3 (shading level is 0.1). Assuming 22 degrees of freedom (one per each year), a correlation of 0.35 is significant at the 95% level using a two-tailed t test. (b) As in (a) except for 30–90-day filtered 850-mb zonal wind variance regressed onto $[\text{OLR}_{\text{EWVS}}^2]$. The contour interval for zonal wind variance is $1 \text{ m}^2 \text{ s}^{-2}$.

activity into the central Pacific, typically associated with ENSO, is evident.

b. Relation with ENSO

This is not to say that ENSO does not impact MJO activity. To see the impact of ENSO on MJO activity, and on intraseasonal convection in general, regressions onto the Niño3 SST index are formed. Figure 9a displays the regression of seasonal mean intraseasonally filtered OLR variance onto Niño3 SST. During warm ENSO episodes, enhanced intraseasonal convective variance tends to occur in the central and eastern Pacific with decreased variance across the eastern Indian Ocean and Indonesia (see also Fink and Speth 1997). Such an anomaly pattern is tantamount to an eastward shift of the intraseasonal convective variance from its normal position in the western Pacific. An eastward shift of coherent eastward-propagating intraseasonal activity (i.e., MJO activity) also occurs (Fig. 9b), but these anomalies are relatively weak compared to the interannual fluctuations that occur at the center of maximum eastward-propagating variance over the Indian and western Pacific Oceans (Fig. 2b). However, the eastward shift during ENSO may still have important dynamical consequences (e.g., Kessler et al. 1995).

The eastward shift during ENSO of both coherent eastward-propagating MJO activity and broadband intraseasonal convective variance is also consistent with that found for 40–50-day zonal wind variance by Gutzler (1991) at a number of stations in the western Pacific. His result is confirmed here by regression of seasonal mean variance of intraseasonally filtered 850-mb zonal

wind onto Niño3 SST (Fig. 9c). Decreased intraseasonal zonal wind variance occurs over Indonesia and the Indian Ocean, and a more modest increase in variance occurs centered on the date line.

Together with this relatively weak signal of an eastward shift of MJO activity during ENSO, the overall level of MJO activity is found to be weakly inversely related to ENSO. Correlations between Niño3 SST (time series shown at bottom of Fig. 5) and the indexes of eastward-propagating convection and 850-mb zonal wind (Table 2) are modestly negative (~ -0.2) and are more moderately negative for the zonal mean 200-mb zonal wind index (-0.34). However, examination of the time series reveals that these negative correlations result mainly from the marked decrease in MJO activity during the two exceptional warm events in 1982/83 and 1997/98. In fact, correlations between the MJO indices and Niño3 SST are essentially zero if these two large warm events are removed from the record (Table 2). That is, some of the remaining warm events show increased activity (1987/88 and 1991/92) and some show decreased activity (1986/87 and 1994/95). Furthermore, cold events show both increased activity (1984/85) and decreased activity (1975/76).

The above analysis suggests that interannual variations of the level of MJO convective activity occur largely independent of ENSO, except during exceptional warm events when MJO convective activity is diminished. An eastward shift of both broadband intraseasonal activity and coherent eastward-propagating activity does occur during warm ENSO episodes, but this eastward displacement does not necessarily occur with a systematic increase or decrease in overall activity.

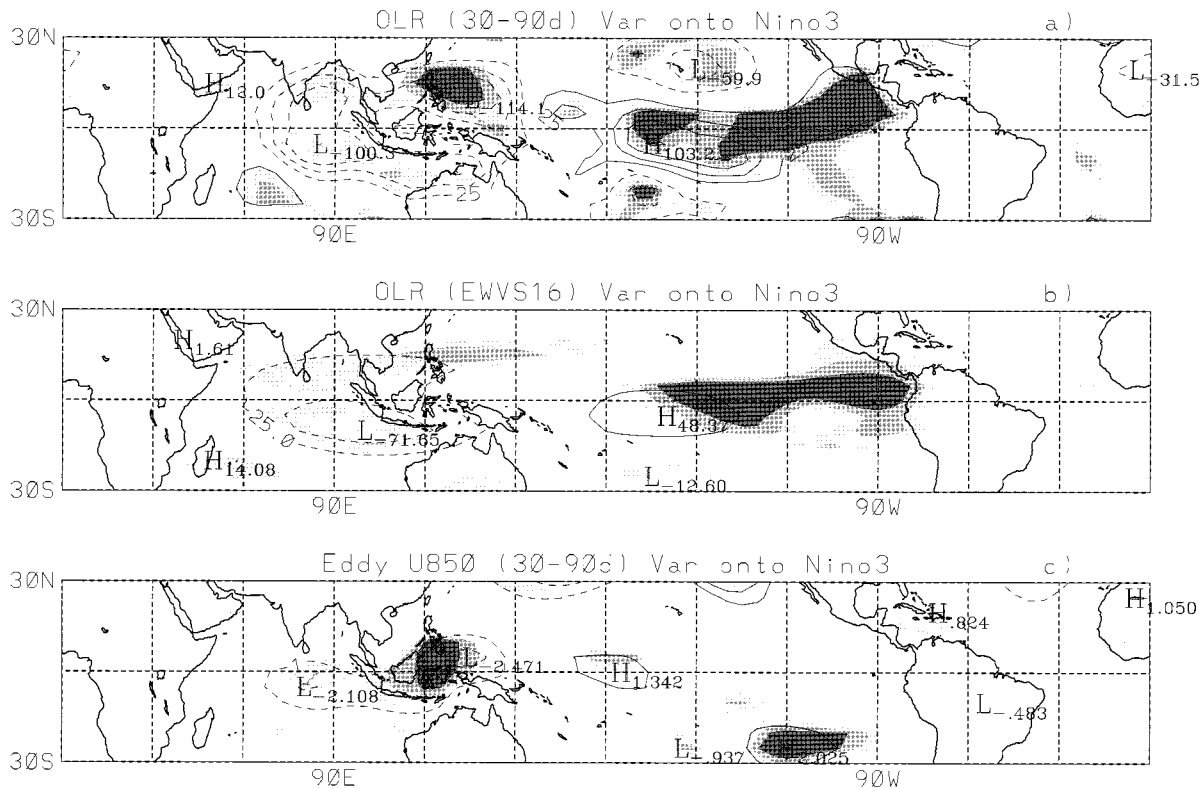


FIG. 9. (a) Regression of Nov–Mar mean 30–90-day filtered OLR variance onto Niño3 SST. (b) Regression of OLR_{EWVS} onto Niño3 SST. Plotting convention is as in Fig. 8a. (c) Regression of 30–90-day filtered 850-mb zonal wind variance onto Niño3 SST. Plotting convention is as in Fig. 8b.

c. Relation with other SST variability

The question is thus raised as to what is responsible for producing the marked interannual variability of the level of MJO activity. The possible relationship with other SST anomalies, besides those related to ENSO, is explored by considering the regression of austral summer mean SST onto $[OLR_{EWVS}^2]$ (Fig. 10). Enhanced MJO activity occurs in conjunction with colder than normal SST in the equatorial eastern Pacific and with warmer than normal SST in the eastern Indian and western Pacific Oceans. However, none of these correlations is large, implying that interannual variations of MJO activity are not strongly related to interannual SST var-

iations (see also Slingo et al. 1999). The SST anomalies in the eastern Pacific in Fig. 10 are related to weaker MJO activity during the two large warm ENSO events of 1982/83 and 1997/98. The weak correlations and magnitudes of the regressed anomalies in the eastern Pacific (only about a 0.25°C anomaly while a typical ENSO anomaly is ~2°C) imply, again, that the overall relationship with ENSO is weak. The warm anomalies in the Indian and western Pacific (only about 0.125°C per standard deviation of $[OLR_{EWVS}^2]$) may, however, actually be relevant for changes in convective activity there, as they occur on top of the already very warm temperatures in the warm pool.

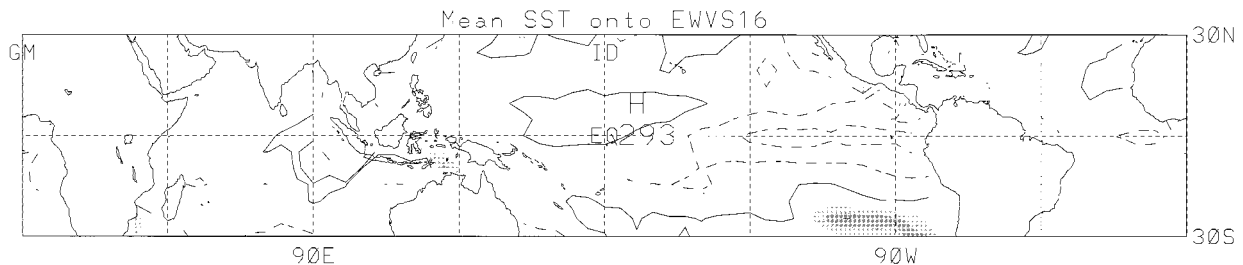


FIG. 10. Regression of Nov–Mar mean SST onto $[OLR_{EWVS}^2]$. Contour interval in is 0.25°C with first contour at 0.125°C. Shading indicates magnitude of the correlation between SST and $[OLR_{EWVS}^2]$ as in Fig. 8.

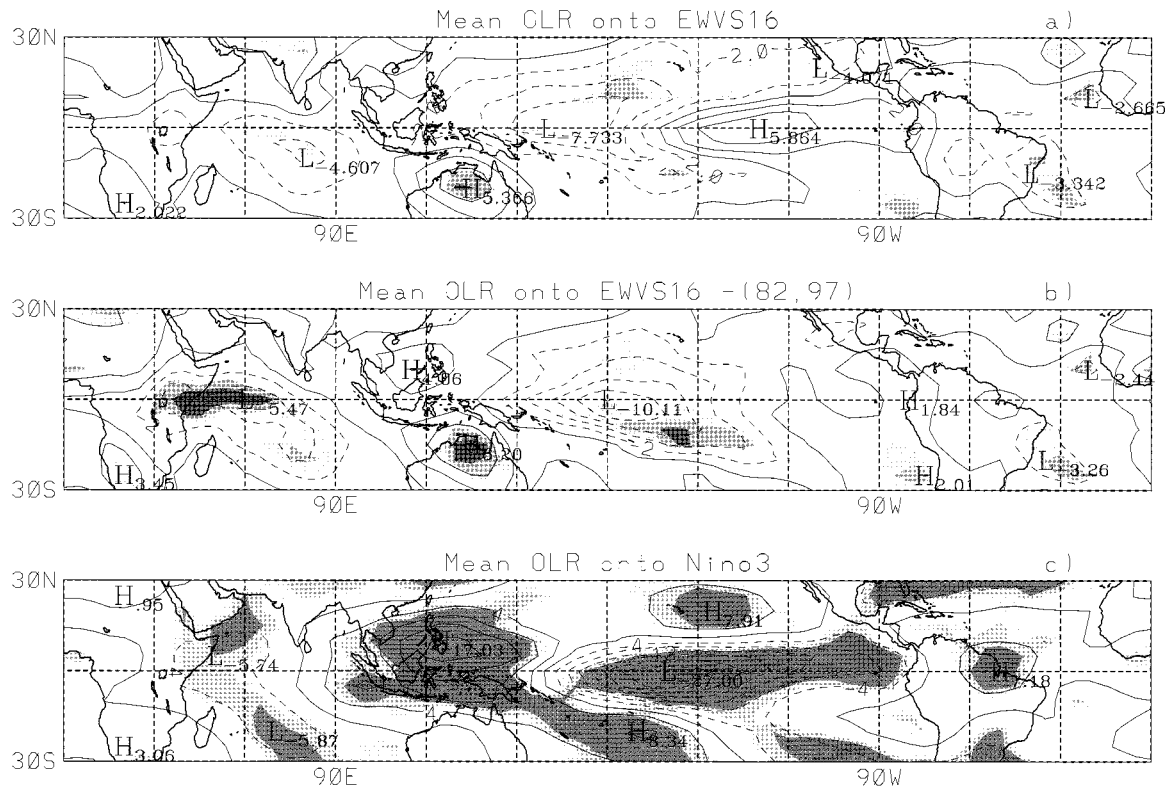


FIG. 11. (a) Regression of Nov–Mar mean OLR onto $[\text{OLR}_{\text{EWVS}}^2]$. Contour interval is 2 W m^{-2} . Shading indicates magnitude of the correlations between mean OLR and $[\text{OLR}_{\text{EWVS}}^2]$ as in Fig. 8. (b) As in (a) except that the exceptional warm ENSO years 1982–83 and 1997–98 are excluded. (c) As in (a) except for summer mean OLR regressed onto Niño3 SST [contour interval 4 W m^{-2} , which is double that in (a) and (b)].

d. Relation with distribution of mean convection

The distribution of mean convection in a particular austral summer may also reflect conditions that impact the level of MJO activity. Figure 11a displays the linear regression of austral summer mean OLR onto the time series of $[\text{OLR}_{\text{EWVS}}^2]$. Enhanced MJO activity occurs in conjunction with enhanced convection (negative OLR anomalies) over equatorial Africa, the equatorial western Indian Ocean, and the equatorial Pacific near the date line, and in conjunction with suppressed convection over northern and central Australia and the eastern Pacific. This pattern is consistent with that for SST (Fig. 10), with enhanced mean convection occurring over the warm SST anomalies. Again, the occurrence of positive OLR anomalies in the eastern Pacific reflects behavior from the two large warm events of 1982/83 and 1997/98, when MJO activity was suppressed in conjunction with large negative OLR anomalies there. If these 2 yr are removed from the record (Fig. 11b), the positive OLR anomalies disappear. The distribution of anomalous mean convection that accompanies enhanced MJO activity is now vaguely similar to that which occurs during a canonical warm ENSO event, with negative convective anomalies in the central Pacific and western

Indian Oceans, and positive OLR anomalies at the longitudes of Indonesia and Australia (Fig. 11c). However, besides the fact that the correlation between MJO activity and Niño3 SST is near zero, even when the two large warm events are removed (Table 2), there are some important differences between the anomalous OLR during years of enhanced MJO activity and during warm ENSO events. Enhanced MJO activity occurs in conjunction with positive OLR anomalies over northern and central Australia, while during ENSO, the positive OLR anomalies are largely confined to north of the continent (Fig. 11c; see also McBride and Nicholls 1983). Also, enhanced MJO activity is associated with enhanced convection extending across equatorial Africa and Brazil, while during ENSO decreased convection occurs over Brazil.

e. Discussion

The level of MJO activity each year varies predominantly independent of anomalous SST, particularly that associated with ENSO. MJO activity does tend to shift eastward during warm ENSO episodes, but the level of activity is not systematically affected except during ex-

ceptional warm events, when it decreases. Years of enhanced MJO activity do, however, display coherent distributions of anomalous mean convection. The net effect of these anomalies of mean OLR during years of enhanced MJO activity is to make the distribution of climatological convection along and just to the south of the equator more uniform from Africa eastward to about 150°W. During large ENSO events the near-continuous distribution of equatorial convection from Africa to the date line is disrupted, with suppressed conditions developing to the north of Australia in conjunction with the eastward shift of convection past the date line. Enhanced MJO activity thus occurs with an “improvement” of conditions conducive to the MJO in the region where the MJO normally occurs (Africa to the date line). Enhanced MJO activity does not seem to be favored by large disruptions to these favorable near-equatorial conditions, either due to large longitudinal shifts of the areas of mean convection as a result of ENSO, or to meridional shifts (for reasons unknown) over Australia (Fig. 11).

5. Summary and conclusions

Measures of MJO activity, the dominant mode of intraseasonal variability in tropical convection, were developed in order to assess the interannual variation of organized, eastward-propagating intraseasonal convection during extended austral summer (November–March) 1974–98. One measure was based on wavenumber-frequency filtering and another was based on EOF analysis. Both of these measures were created for OLR as well as for the zonal wind at 850 mb. All of these measures equally capture the salient properties of the MJO, which include prominent eastward propagation at low planetary wavenumbers and confinement primarily to the Indian and western Pacific Oceans. Comparison was also made to the zonal mean zonal wind index proposed by Slingo et al. (1999). While not all of the variance captured by this index is directly related to the MJO, the general agreement with the explicit indexes of the MJO confirms the utility of this zonal wind index, especially considering its simplicity.

An increase in the level of MJO activity primarily occurs in conjunction with an increase in the number of discrete MJO events each year. Enhanced MJO activity also occurs in conjunction with enhanced intraseasonal convective activity across the Indian and western Pacific Oceans, which is where the MJO is normally prominent. Years of enhanced MJO activity also tend to have longer-period MJOs. Year-to-year variations in the level of MJO activity are not strongly related to significant eastward excursions of convective variance into the central Pacific, such as occurs during ENSO. However, enhanced MJO activity does tend to occur in conjunction with an increase in contiguous mean convection from equatorial Africa to just east of the date line. Such anomalies do not appear to be strongly related

to SST anomalies. Nonetheless, MJO formation presumably is favored by such zonally contiguous, near-equatorial convection (e.g., Wang and Li 1994; Salby et al. 1994), which, for instance, can also explain why the seasonal cycle of MJO activity peaks during austral summer and not during boreal summer when the Asian–Indian monsoon is active well off the equator (e.g., Salby and Hendon 1994). The tendency for years of enhanced MJO activity to have MJOs with longer periods is also consistent with the tendency for enhanced MJO activity to occur in conjunction with an increase in contiguous mean equatorial convection across the Eastern Hemisphere. Presumably, in those years when contiguous equatorial convection is more zonally uniform, the coupling of the dynamical components of the MJO with convection, during which time the MJO moves at a slower phase speed than when the convective component is absent (e.g., Hendon and Salby 1996), occurs over a greater range of longitude and for a greater duration, hence leading to a longer period.

Interannual variation of the level of MJO activity during austral summer was found to exhibit little systematic relationship with ENSO, except during extremely large warm events when MJO activity is suppressed. Displacement of intraseasonal convective variance east of the date line does occur during warm events (see also Gutzler 1991; Fink and Speth 1997) and may have important dynamical consequences (e.g., Kessler et al. 1995), but such a displacement appears not to affect a change in the overall level of eastward-propagating, spatially coherent activity. The lack of a clear signal in the intensity of the MJO during the nonstrong ENSO events probably stems from the fact that, in some ENSO events, the distribution of near-equatorial convection from Africa to the date line is not totally disrupted, and favorable near-equatorial conditions for the formation of the MJO then span a greater range of longitudes.

That interannual variability of MJO activity is not too strongly related to any other SST anomalies suggests that most of the year-to-year variability is internally generated independent of any slowly varying boundary forcing. Analyses of an ensemble of global climate model integrations have led to similar conclusions (Slingo et al. 1999). This independent interannual variability of convection associated with the MJO, especially in the sensitive equatorial central Pacific (e.g., Fig. 11b), may, however, play an important role in limiting predictions of the climate system, which are based solely on anomalous equatorial Pacific SSTs.

While no strong observational relationship between the level of MJO activity and SST exists, the apparent inverse relationship with the mean Australian summer monsoon (Fig. 11a) may be of practical significance. Enhanced MJO activity tends to occur in conjunction with a weakened monsoon over continental Australia (see also Holland 1986). Although this relation is similar to that which occurs during warm phases of ENSO (McBride and Nicholls 1983), the reduction of monsoon

convection associated with enhanced MJO activity covers more of the continent and is largely independent of ENSO. Such rainfall variations associated with the MJO, but independent of ENSO, may help explain why the negative correlation between ENSO and monsoon rainfall is weakest during the peak of the summer wet season (McBride and Nicholls 1983). It is during this time that the MJO is most active and hence exerts the most influence on northern Australia.

Acknowledgments. The comments of the anonymous reviewers and the editor, Neville Nicholls, led to significant improvements in the manuscript. This work was supported by the GOALS Program of NOAA/OGP.

REFERENCES

- Anyamba, E. K., and B. C. Weare, 1995: Temporal variability of the 40–50 day oscillation in tropical convection. *Int. J. Climatol.*, **15**, 379–402.
- Ferranti, L., T. N. Palmer, F. Molteni, and E. Klinker, 1990: Tropical–extratropical interaction associated with the 30–60 day oscillation and its impact on medium and extended range prediction. *J. Atmos. Sci.*, **47**, 2177–2199.
- Fink, A., and P. Speth, 1997: Some potential forcing mechanisms of the year-to-year variability of the tropical convection and its intraseasonal (25–70 day) variability. *Int. J. Climatol.*, **17**, 1513–1534.
- Gadgil, S., and G. Asha, 1992: Intraseasonal variations of the Indian summer monsoon. Part I: Observational aspects. *J. Meteor. Soc. Japan*, **70**, 517–527.
- Gutzler, D. S., 1991: Interannual fluctuations of intraseasonal variance of near-equatorial zonal winds. *J. Geophys. Res.*, **96**, 3173–3185.
- , and R. A. Madden, 1989: Seasonal variations in the spatial structure of intraseasonal tropical wind fluctuations. *J. Atmos. Sci.*, **46**, 641–660.
- Hendon, H. H., 1995: Length of day changes associated with the Madden–Julian oscillation. *J. Atmos. Sci.*, **52**, 2373–2383.
- , and B. Liebmann, 1990: A composite study of onset of the Australian summer monsoon. *J. Atmos. Sci.*, **47**, 2227–2240.
- , and M. L. Salby, 1996: Planetary-scale circulations forced by intraseasonal variations of observed convection. *J. Atmos. Sci.*, **53**, 1751–1758.
- , B. Liebmann, and J. D. Glick, 1998: Intraseasonal Kelvin waves and the Madden–Julian oscillation. *J. Atmos. Sci.*, **55**, 88–101.
- Holland, G. J., 1986: Interannual variability of the Australian summer monsoon at Darwin: 1952–82. *Mon. Wea. Rev.*, **114**, 594–604.
- Kalnay, E., and Coauthors, 1996: The NCEP/NCAR 40-Year Reanalysis Project. *Bull. Amer. Meteor. Soc.*, **77**, 437–471.
- Kessler, W. S., M. J. McPhaden, and K. M. Weickmann, 1995: Forcing of intraseasonal Kelvin waves in the equatorial Pacific Ocean. *J. Geophys. Res.*, **100**, 613–631.
- Lau, K.-M., and P. H. Chan, 1986: Aspects of the 40–50 day oscillation during the northern summer as inferred from outgoing longwave radiation. *Mon. Wea. Rev.*, **114**, 1354–1367.
- , and —, 1988: Intraseasonal and interannual variations of tropical convection: A possible link between the 40–50 day oscillation and ENSO? *J. Atmos. Sci.*, **45**, 506–521.
- Liebmann, B., and C. A. Smith, 1996: Description of a complete (interpolated) outgoing longwave radiation dataset. *Bull. Amer. Meteor. Soc.*, **77**, 1275–1277.
- Madden, R. A., 1986: Seasonal variations of the 40–50 day oscillation in the tropics. *J. Atmos. Sci.*, **43**, 3138–3158.
- , and P. R. Julian, 1972: Description of global-scale circulation cells in the tropics with a 40–50 day period. *J. Atmos. Sci.*, **29**, 1109–1123.
- McBride, J. L., and N. Nicholls, 1983: Seasonal relationships between Australian rainfall and the Southern Oscillation. *Mon. Wea. Rev.*, **111**, 1998–2004.
- North, G. R., T. L. Bell, R. F. Cahalan, and F. J. Moeng, 1982: Sampling errors in the estimation of empirical orthogonal functions. *Mon. Wea. Rev.*, **110**, 699–706.
- Ralph, E. A., K. Bi, and P. P. Niiler, 1997: A Lagrangian description of the western equatorial Pacific response to the wind burst of December 1992. *J. Climate*, **10**, 1706–1721.
- Reynolds, R. W., and T. M. Smith, 1994: Improved global sea surface temperature analyses using optimum interpolation. *J. Climate*, **7**, 929–948.
- Salby, M. L., and H. H. Hendon, 1994: Intraseasonal behavior of clouds, temperature, and winds in the Tropics. *J. Atmos. Sci.*, **51**, 2207–2224.
- , R. R. Garcia, and H. H. Hendon, 1994: Planetary-scale circulations in the presence of climatological and wave-induced heating. *J. Atmos. Sci.*, **51**, 2344–2367.
- Slingo, J. M., D. P. Rowell, K. R. Sperber, and F. Nortley, 1999: On the predictability of the interannual behaviour of the Madden–Julian oscillation and its relationship with El Niño. *Quart. J. Roy. Meteor. Soc.*, in press.
- Smith, T. M., R. W. Reynolds, R. E. Livezey, and D. C. Stokes, 1996: Reconstruction of historical sea surface temperatures using empirical orthogonal functions. *J. Climate*, **9**, 1403–1420.
- Wang, B., and H. Rui, 1990: Synoptic climatology of transient tropical intraseasonal convective anomalies: 1975–1985. *Meteor. Atmos. Phys.*, **44**, 43–61.
- , and T. Li, 1994: Convective interaction with boundary-layer dynamics in the development of a tropical intraseasonal system. *J. Atmos. Sci.*, **51**, 1386–1400.
- Weickmann, K. M., G. R. Lussky, and J. E. Kutzbach, 1985: Intraseasonal (30–60 day) fluctuations of outgoing longwave radiation and 250 mb streamfunction during northern winter. *Mon. Wea. Rev.*, **113**, 941–961.
- Zhang, C., and H. H. Hendon, 1997: Propagating and standing components of the intraseasonal oscillation in tropical convection. *J. Atmos. Sci.*, **54**, 741–752.